Structure of multi-wall carbon nanotubes

AIP | Applied Physics Letters

Structure of multi-wall carbon nanotubes: AA stacked graphene helices

Jae-Kap Lee, Sohyung Lee, Yong-Il Kim, Jin-Gyu Kim, Kyung-Il Lee, Jae-Pyoung Ahn, Bong-Ki Min, Chung-Jong Yu, Keun Hwa Chae, and Phillip John

Citation: Applied Physics Letters **102**, 161911 (2013); doi: 10.1063/1.4802881
View online: http://dx.doi.org/10.1063/1.4802881
View Table of Contents: http://scitation.aip.org/content/aip/journal/apl/102/16?ver=pdfcov
Published by the AIP Publishing

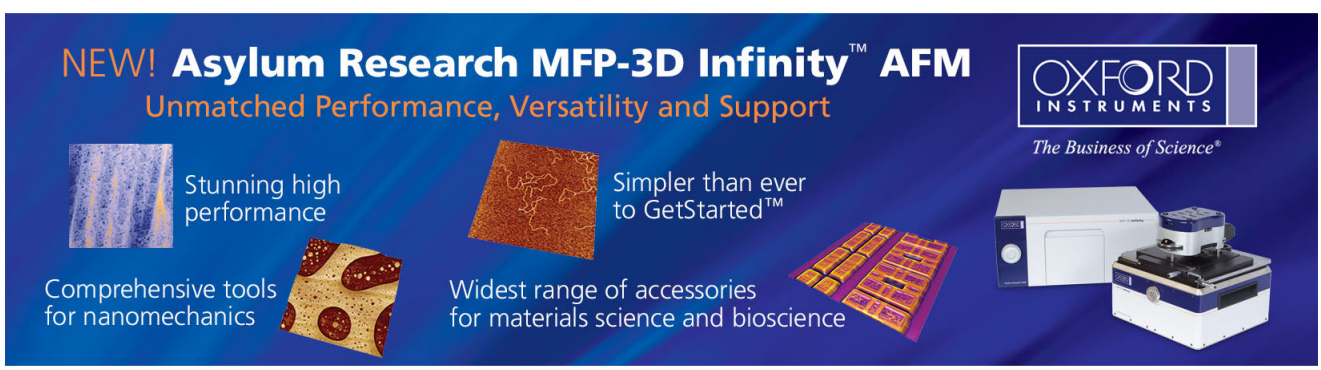

Structure of multi-wall carbon nanotubes: AA′ stacked graphene helices

Jae-Kap Lee,[1,a)] Sohyung Lee,[1,2] Yong-Il Kim,[3] Jin-Gyu Kim,[4] Kyung-Il Lee,[5] Jae-Pyoung Ahn,[6] Bong-Ki Min,[7] Chung-Jong Yu,[8] Keun Hwa Chae,[6] and Phillip John[9]
[1]*Surface Control Research Center, Korea Institute of Science and Technology, Seoul 130-650, South Korea*
[2]*Department of Semiconductor Science, Dongguk University, Seoul 100-715, South Korea*
[3]*Division of Metrology for Quality of Life, Korea Research Institute of Standards and Science, Daejeon 305-600, South Korea*
[4]*Division of Electron Microscopic Research, Korea Basic Science Institute, Daejeon 305-340, South Korea*
[5]*Nano-Bio Division, Nuri Vista Co. Ltd., Incheon 406-840, South Korea*
[6]*Analysis Center, Korea Institute of Science and Technology, Seoul 130-650, South Korea*
[7]*Instrumental Analysis Center, Yeungnam University, Daegu 712-749, South Korea*
[8]*Division of Science and Technology, Pohang University, Pohang 790-784, South Korea*
[9]*School of Engineering and Physical Sciences, Heriot-Watt University, Edinburgh EH14 4AS, United Kingdom*

(Received 25 January 2013; accepted 21 March 2013; published online 24 April 2013)

The structure of multi-wall carbon nanotubes has been attributed previously to disordered stacking of the graphene planes. Evidence is presented that the nanotubes analyzed in this paper occur with stacked graphene layers in the sequence of AA′, where alternate graphene planes are translated by half the hexagon width. We further present proof that the crystalline materials comprise graphene helices (∼5 nm in width), rather than in the form of a perfect tube. We also show that the structural model proposed here may be a common structure for multi-wall carbon nanotubes. © *2013 AIP Publishing LLC* [http://dx.doi.org/10.1063/1.4802881]

With their unique features and resulting diverse properties, multi-wall carbon nanotubes (MWNTs) are of worldwide interest, and numerous studies have been performed since the first report of their synthesis in 1991.[1] Nevertheless, to date, the specific structure of MWNTs is still uncertain, and no single model is capable of addressing the various kinds of morphologies reported. There are two main types of structural models, concentrically nested tubes and a scroll of graphene sheets (or the coexistence of the two forms).[2–6] Although the premise of the two models is the disordered stacking of graphene sheets, a few groups[7–9] have suggested the existence of an intermediate state between crystalline AB graphite and the turbostratic stacking based on signals assigned to the hexagonal (100) and (110) planes together with the (002) plane in X-ray,[7,10–15] electron,[1,3,8,15–26] and neutron[9,27] diffraction analysis. This feasible suggestion has not gained ground because a relevant structure could not be analytically proven whilst others attributed the appearance of the signals to regular chirality of the disordered graphene sheets or the structural diversity of graphitic materials.

Previously, we have shown that the AA′ stacking of graphene layers, in which alternate graphene planes are translated by a half width of the hexagon, appears together with AA stacked graphite on diamond (111) surfaces due to the symmetry of the unreconstructed diamond (111) plane.[28] The theoretical spacing of the AA′ stacking was approximately 3.43 Å,[28] which is very close to that normally measured from MWNTs, i.e., about 3.44 Å.[1,7,10–13] The total energy per atom for the AA′ stacking, −40.44 eV/atom, lies between that of AB (lowest) and AA (highest) stacking, although the difference is small at ∼10 meV per atom.[28] This calculation suggests that AA′ graphite may be observed under conditions where the rate of formation is kinetically controlled. Nevertheless, the structure and the characteristic AA′ stacking have not been previously observed.

In this paper, we analyze the crystallographic structure of the AA′ stacking of graphene layers and show that the conventional MWNT samples characterized here[29] are composed of AA′ stacked graphene helices. We also discuss that our structure model can explain the experimental data of MWNTs in the literature.

Figure 1 shows the crystal structure of AA′ graphite, assigned to an orthorhombic *Fmmm* (#69) space group, unlike AB[29] or AA graphite which are assigned to a hexagonal group.[30] The simulated X-ray diffraction (XRD) pattern of AA′ graphite is very similar to that of AB graphite (Fig. 2(a)), in which the allowed reflections, 002, 020, 111, 022, 004, 113, 024, 200, 131, 202, 133, 040, and 222 peaks are predicted. The key differences lie in the appearance of 131 and 133 peaks.

XRD patterns of vapor phase catalytic chemical vapor deposition (VCCVD)- and arc-MWNTs show the unique feature[7,10–15] that two strong peaks at $2\theta \approx 42°$ (d-value = 2.13 Å) and $2\theta \approx 77°$ (d-value = 1.23 Å) appear, together with the dominant 002 ($2\theta \approx 25.9°$, d-value = 3.44 Å) and 004 peaks, as shown in Fig. 2(b). The 020 and 200 peaks of arc-MWNTs are very sharp, corresponding to those of crystalline graphite.[10] Indeed, the XRD patterns well fit with the predicted pattern[31] for ⟨001⟩ oriented AA′ graphite (the tubular material can be regarded as a thin graphite film (Fig. 3)) where 002 and 020 peaks become relatively stronger. The interplanar spacing, 3.44 Å, measured from each 002 peak of arc- and VCCVD-MWNTs, is close to the theoretical value of the AA′ stacking, 3.43 Å.[28] The results indicate that the materials are crystalline comprising ⟨100⟩ oriented AA′ graphene layers.

The electron diffraction (ED) pattern measured from an arc-tubule, which was not tilted (i.e., the inclination

[a)]Author to whom correspondence should be addressed. Electronic mail: jklee@kist.re.kr

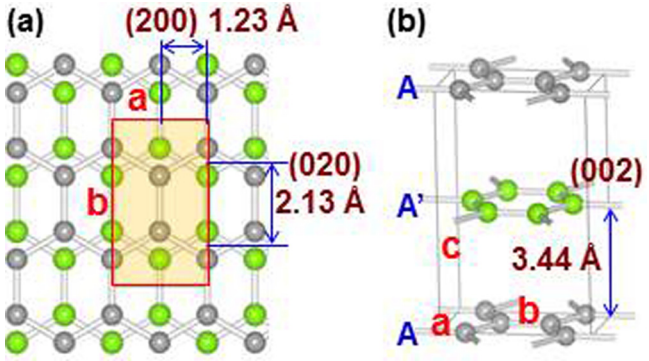

FIG. 1. Crystal structure of AA′ graphite. (a) The plan view of AA′ graphite (orthorhombic, $a = 2.46$ Å, $b = 4.26$ Å, $c = 6.88$ Å, angles = all 90°). (b) The primitive cell of AA′ graphite.

angle,[15,16] $\beta = 0$) on the horizontal line of the TEM grid, is identical to the expected pattern for the AA′ crystal in a zigzag structure, as shown in Fig. 4(b). The pattern is interpreted in terms of the orthorhombic AA′ unit cell although much weaker h100 and h110 spots, which are related with the hexagonal AB structure and 113 spots, appear. A clearer ED pattern obtained from different sample (Fig. 4(c)) shows evidence that the tubule was tilted by 3°. The spots of (020) and (200) planes, which are not parallel to the tubule axis, are split into two and appear as a pair of spots. From a tubule tilted by 10°, another pair of 020 and 200 spots appear on Ewald's spheres (Fig. 4(d)). Also, the spots of the unique 131 plane of the AA′ crystal, which is oriented by 11° to the beam direction (Fig. 3(c)), ⟨001⟩, are evident. The data provide evidence that the arc-MWNTs adopt an AA′ zigzag configuration.

Many ED patterns that are similar to those shown in Figs. 4(b)–4(d) have been reported for MWNTs,[1,3,15–26] including double-wall CNTs,[17,18] mainly prepared by the arc discharge or the ACCVD (i.e., aligned catalytic CVD growth on a substrate) technique. Previous researchers have interpreted the ED patterns as the disordered stacking of graphene layers with uniform chirality. However, such ED patterns, where 020 and 200 spots coexist with 002 and 004 spots, cannot appear in the turbostratic stacking with any regularity.[29] Particularly, the

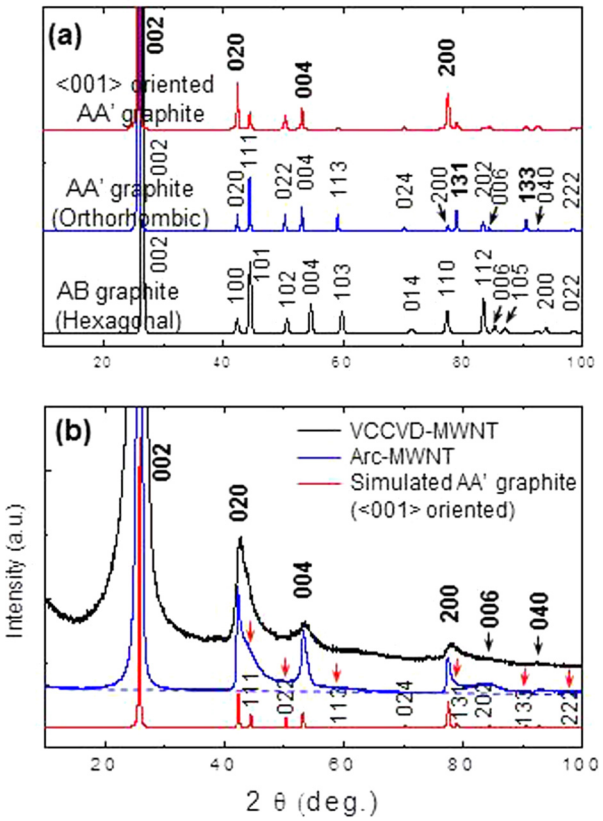

FIG. 2. (a) Simulated XRD patterns ($\lambda = 1.541$ Å) of AB graphite, AA′ graphite ($c = 6.88$ Å), and ⟨001⟩ oriented AA′ graphite. The simulation for the oriented AA′ graphite was performed using the modified March-Dollas function in the RIETAN-FP program (see Ref. 31). (b) XRD patterns of purified arc- and VCCVD-MWNTs.

split ED signals, originating from the inclination tilts of the samples on the TEM grid which cannot be controlled,[15] were interpreted as evidence of chirality.[1,3,15–26] The ED pattern for the armchair structure[29] has neither been reported in the literature nor observed in this study. The relatively larger angle to the tubule axis, leading to a steeper curvature of the graphene ribbons, makes the armchair structure energetically unfavorable; the calculated strain energy[32] of graphene ribbons in the zigzag configuration is about one-third that of those of the

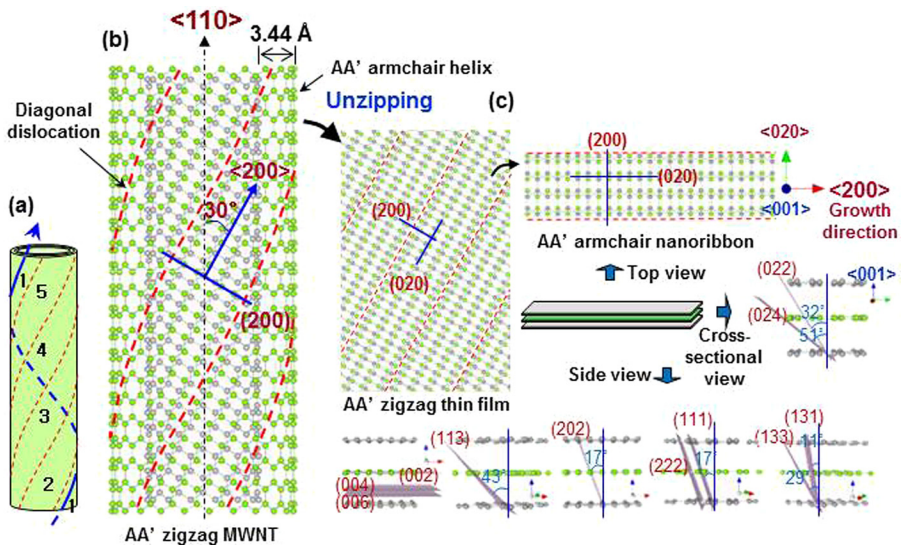

FIG. 3. (a) and (b) A model of MWNTs. MWNTs are of tubular construction of the AA′ armchair graphene helices, forming a zigzag configuration (b) (semitube). The blue line in (a) indicates the track of graphene helix 1. (c) Schematic diagrams simplifying the structure of MWNTs as a ⟨001⟩ oriented AA′ zigzag graphene thin film and showing the reflection planes of the AA′ crystal.

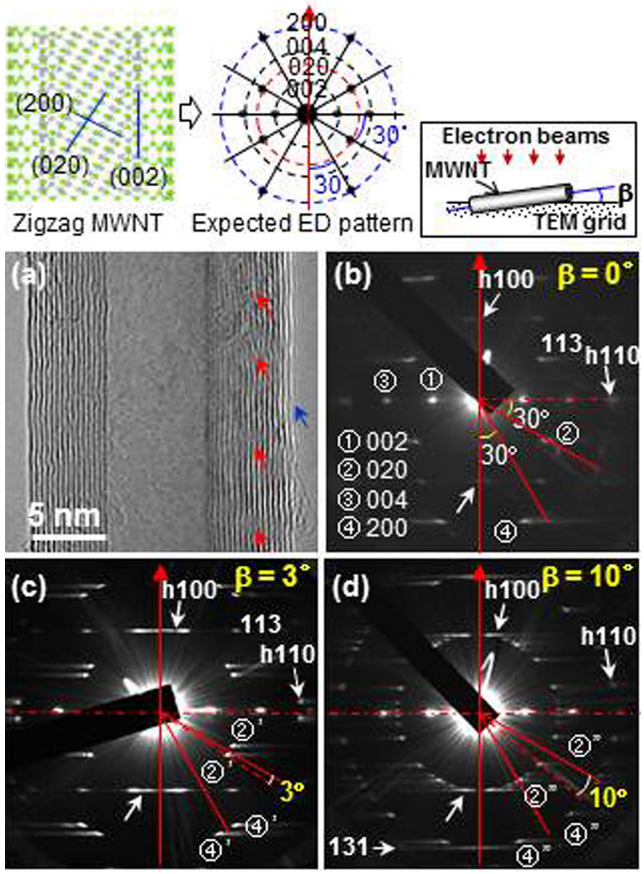

FIG. 4. ED pattern analysis of arc-MWNTs. (a) A HRTEM image of an arc-MWNT. (b)-(d) ED patterns measured from individual MWNT. The inset is a schematic diagram explaining the inclination angle (β) of the sample on the TEM stage.

armchair configuration. The results of ED analysis indicate that the AA′ stacked zigzag configuration is a common structure of MWNTs.

The critical question is how the AA′ stacking can be retained in the tubular material where the structure is commonly known as concentric graphene layers with different diameters. The helical growth of narrow but long graphene sheets provide a solution to the problem. The unique AA′ stacking of armchair graphene ribbons can cause the helical growth when the (200) plane, which is the closest-packed plane, appears at an angle to tubule axis. Here, ⟨200⟩ becomes the preferential growth direction which drives the helical growth of the armchair graphene ribbons, resulting in the zigzag tubule where the angle of ⟨200⟩ with respect to the tubule axis is 30° (Fig. 3(b)).

Graphene helices, which appear as a stack, are detectable with high-resolution transmission electron microscopy (HRTEM) tilt experiments, as shown in Fig. 5. The VCCVD-tubule reveals the stacked graphene helices (the yellow arrows in Fig. 5(a)) in the curved part (such morphology prevails in the literature).[25,33–38] With 40° tilt of the sample stage, the straight part of the VCCVD-tubule reveals the stacked graphene helices (the red arrows in Fig. 5(a′)), and the angle of the helices to the tubule axis (the yellow arrows in Fig. 5(a′)) becomes steep and is measured to be about 30°. The analysis indicates that the stacked graphene helices of the tubule lie at an angle of 30° to the tubule axis.

The profile of the graphene helices is evident in the AFM image obtained from a VCCVD-tubule (Figs. 6(a) and 6(b)) where the tubule with the diameter of ≈20 nm (Ref. 29) appears to be broadened (≈110 nm in width) due to the AFM tip effects. The angles of the helices to the tubule axis ranging 64°–72° in the distorted image span 21°–29° in the corrected image. The line scan data indicate that the heights between the graphene helices (plateaus in the line scan) are one or two atomic thicknesses (0.4–0.8 nm). The atomic height steps in AFM data are due to the incoherent scroll of the blocked graphene helices (Fig. 6(b)), resulting in the typical herring-bone morphology of VCCVD-MWNTs.[39] The HRTEM and AFM analyses (Figs. 5 and 6) demonstrate that the tubular materials are composed of stacked graphene helices (with a thickness of ∼5 nm, corresponding to the thickness of the wall of the VCCVD tubule) subtending an angle

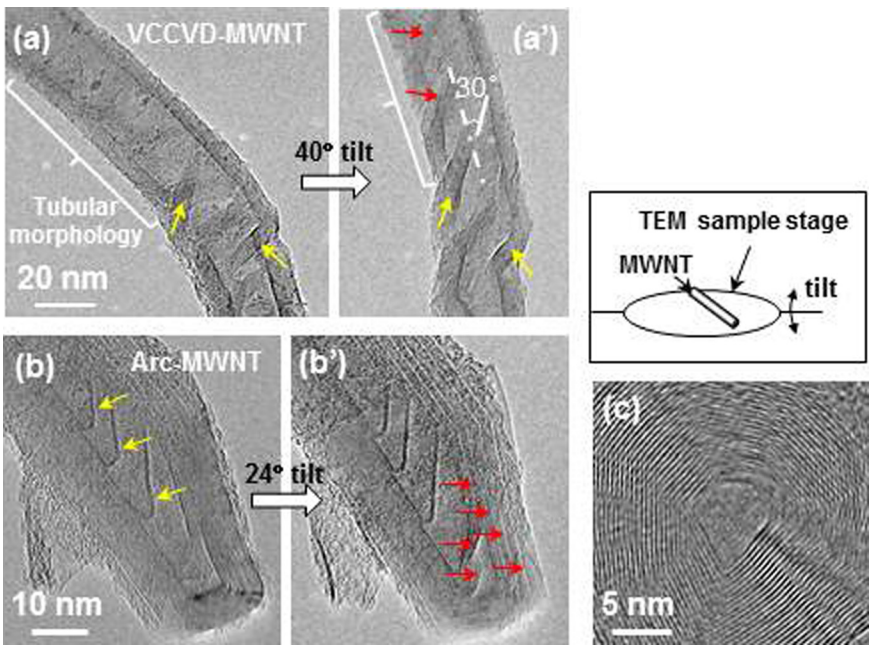

FIG. 5. HRTEM images of a VCCVD-MWNT (a, a′) and an arc-MWNT (b, b′) with tilts. (c) A cross-section of an arc-MWNT revealing polygonized morphology. The yellow and red arrows indicate the stacked graphene helices.

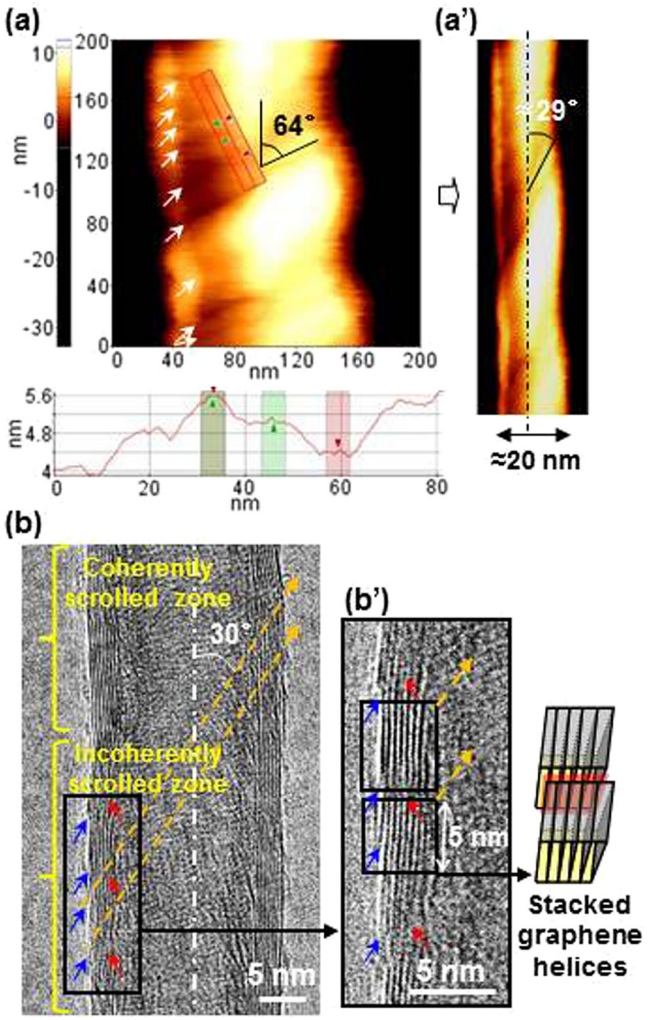

FIG. 6. AFM and HRTEM images of VCCD-MWNTs. A non-contact-mode AFM image of a VCCVD-MWNT (a) and its corrected image (a′). A HRTEM image of a VCCVD-MWNT. The superimposed dotted arrows on the tubule (b, b′) indicate the imaginary tracks of the graphene helices subtending an angle of 30° to the tubule axis.

of 30° to the tubule axis. On the other hand, probing the graphene helices from arc-MWNTs has not been achieved. We attribute this to the typical feature of arc-MWNTs, i.e., comprising coherently scrolled graphene helices (Fig. 4(a)) and the relatively poor spatial resolution of AFM.

The bamboo and closed ends structures[2,4–6,33–43] shown in Fig. 5(b), which prevail in arc- as well as CVD-MWNTs, are evidence of our graphene helices model. Due to the imaging mechanism of TEM, the tubules with locally released graphene helices inside and at the ends of tubules can be seen as the bamboo or capped structures, respectively. The polygonized (graphite-like) morphology is evident in the cross-sectional image of an arc-MWNT (Fig. 5(c)). The helical and polygonized structure of MWNTs explains the appearance of the unexpected h100 and h110 signals of the AB structure (Figs. 4(b)–4(d)). The stacked graphene nanoribbons easily slide, and this can break the symmetry of the AA′ crystal resulting in revelation of the latent h100 and h110 signals.[29] The polygonized (or distorted) AA′ stacked graphene nanoribbons can reveal the unexpected 113 spots (Figs. 4(b)–4(d)). The current model also explains the periodically blurred lattice fringes (the red arrows) and the disconnected lattices on the surfaces of the tubules (the blue arrows) in Figs. 4(a) and 6(b), which are common in HRTEM[1–6,8,11,12,14,15,20,23–26,33–43] and scanning tunneling microscopy[35] images in the literature.

Thus, in summary, MWNTs are of tubular construction formed by the helical growth of the AA′ stacked armchair graphene ribbons whose widths are on the order of several nm. The crystalline growth resulted in the preferred and nonchiral zigzag configuration as the minimum energy configuration: the calculated strain energy[32] of the graphene helix is one-fourth of that of seamless graphene tubes. We expect that the graphene helices, particularly, comprising the coherently scrolled arc-MWNTs can be locally "zipped up" where atomic matching is ideal, and such samples can be seen as concentrically nested tubes. Our model implies that the properties of MWNTs are dependent on the internal structure of individual MWNT which varies from one tubule to another. This explains the inconsistent physical properties reported for MWNTs[43,44] despite the numerous investigations that have been carried out since 1991.[1] The dramatic conversion of VCCVD-MWNTs with the typical bamboo morphology into graphitic nanoribbons (Fig. 1 of Ref. 45) by mechanical milling supports the proposed model.

The oriented nanocrystalline structure of MWNTs explains the unique XRD patterns which are different from the expected pattern of the orthorhombic crystal (Fig. 2(a)). The tubules, comprising the AA′ stacked armchair graphene nanoribbons, broaden the XRD signals except for the (020) plane which are parallel to the graphene nanoribbons (Fig. 3). This explains the XRD pattern of the VCCVD-MWNTs (mostly incoherently scrolled), where the 020 peak is very strong whilst other peaks, apart from the 002 and 004 peaks, are weak, 200 peak, or absent (Fig. 2(b)). Coherently scrolled arc-MWNTs exhibit strong 200 signal because the 200 planes cross the diagonal dislocations (Fig. 3). This explains the relatively sharp and strong 200 signal of arc-MWNTs, compared with that of VCCVD-MWNTs (Fig. 2(b)), to be associated with different structures depending on the growth conditions. The traces (backgrounds) of the broadened signals, including the unique 131 and 133 peaks of the AA′ crystal, are evident in the arc-MWNT pattern (the red arrows in Fig. 2(b)). The extent of the broadening of the signals may depend on the angles of the reflection planes with respect to ⟨001⟩ and ⟨200⟩ directions of the AA′ crystal as well as the dimension (or curvature) of the graphene nanoribbons (Fig. 3).

Due to the absence of 111, 022, 113, 024, and 202 signals in the typical XRD patterns for MWNTs the material has been interpreted as turbostratic stacking.[10–14] The XRD patterns of carbon black revealing three broad signals reported by Biscoe *et al.* (Fig. 4(a) of Ref. 46) are representative of imperfect turbostratic graphite. The material crystallizes with heat-treatment at ∼3000 °C, resulting in the dramatic change of the morphology from nanoparticles to polygonal graphitic helices.[47] Indeed, the XRD pattern of the polygonal graphitic nanohelices is identical to those of MWNTs with the spacing of 3.44 Å (Fig. 4(c) of Ref. 46) associated with crystalline AA′ graphite. We expect that the ideal spacing of disordered graphite may be ≈3.48 Å, measured from the randomly oriented graphene nanoribbons which were decomposed from VCCVD-MWNTs by

mechanical milling.[45] The conventional interpretation of the structure as turbostratic since 1942 (Ref. 46) is challenged in the present paper.

We thank Wonyong Kim and Kil-joon Min for AFM work; Man-Ho Kim, Kwang-Ryeol Lee, Young-Man Kim, Seung-Cheol Lee, and Young-Su Lee for useful comments on the crystal of AA′ graphite. This work was supported by KIST Future Resource Program (2V01900, 2V02120, and 2E24011).

[1]S. Iijima, Nature (London) **354**, 56 (1991).
[2]S. Iijima, Mater. Sci. Eng. B **19**, 172 (1993).
[3]W. Ruland, A. K. Schaper, H. Hou, and A. Greiner, Carbon **41**, 423 (2003).
[4]S. Amelinckx, D. Bernaerts, X. B. Zhang, G. Van Tendeloo, and J. Van Landuyt, Science **267**, 1334 (1995).
[5]J. G. Lavin, S. Subramoney, R. S. Ruoff, S. Berber, and D. Tománek, Carbon **40**, 1123 (2002).
[6]S. Q. Feng, D. P. Yu, G. Hu, X. F. Zhang, and Z. Zhang, J. Phys. Chem. Solids **58**, 1887 (1997).
[7]D. Reznik, C. H. Olk, D. A. Neumann, and J. R. D. Copley, Phys. Rev. B **52**, 116 (1995).
[8]M. Liu and J. M. Cowley, Ultramicroscopy **53**, 333 (1994).
[9]A. Burian, J. C. Dore, H. E. Fischer, and J. Sloan, Phys. Rev. B **59**, 1665 (1999).
[10]Y. Saito, T. Yoshikawa, S. Bandow, M. Tomita, and T. Hayashi, Phys. Rev. B **48**, 1907 (1993).
[11]O. Zhou, R. M. Fleming, D. W. Murphy, C. H. Chen, R. C. Haddon, A. P. Ramirez, and S. H. Glarum, Science **263**, 1744 (1994).
[12]H. Yusa and T. Watanuki, Carbon **43**, 519 (2005).
[13]Y. Maniwa, R. Fujiwara, H. Kira, H. Tou, E. Nishibori, M. Takata, M. Sakata, A. Fujiwara, X. Zhao, S. Iijima, and Y. Ando, Phys. Rev. B **64**, 073105 (2001).
[14]W. Z. Zhu, D. E. Miser, W. G. Chan, and M. R. Hajaligol, Mater. Chem. Phys. **82**, 638 (2003).
[15]J.-M. Zuo, T. K. Kim, A. Celik-Aktas, and J. Tao, Z. Kristallogr. **222**, 625 (2007).
[16]X. B. Zhang and S. Amelinckx, Carbon **32**, 1537 (1994).
[17]K. Hirahara, M. Kociak, S. Bandow, T. Nakahira, K. Itoh, Y. Saito, and S. Iijima, Phys. Rev. B **73**, 195420 (2006).
[18]J.-F. Colomer, L. Henrard, G. Van Tendeloo, A. Lucas, and P. Lambin, J. Mater. Chem. **14**, 603 (2004).
[19]Z. Liu, Q. Zhang, and L.-C. Qin, Appl. Phys. Lett. **86**, 191903 (2005).
[20]M. Liu and J. M. Cowley, Carbon **32**, 393 (1994).
[21]D. Bernaerts, S. Amelinckx, Ph. Lambin, and A. A. Lucas, Appl. Phys. A **67**, 53 (1998).
[22]S. Amelinckx, A. A. Lucas, and P. Lambin, Rep. Prog. Phys. **62**, 1471 (1999).
[23]A. A. Lucas, V. Bruyninckx, Ph. Lambin, D. Bernaerts, S. Amelinckx, J. Van Landuyt, and G. Van Tendeloo, Scanning Microsc. **12**, 415 (1998).
[24]Z. Liu and L.-C. Qin, Chem. Phys. Lett. **402**, 202 (2005).
[25]V. P. Dravid, X. Lin, Y. Wang, A. Yee, J. B. Ketterson, and R. P. H. Chang, Science **259**, 1601 (1993).
[26]X. F. Zhang, X. B. Zhang, G. Van Tendeloo, S. Amelinckx, M. Op de Beeck, and J. Van Landuyt, J. Cryst. Growth **130**, 368 (1993).
[27]J. Koloczek, A. Burian, J. C. Dore, and A. C. Hannon, Diamond Relat. Mater. **13**, 1218 (2004).
[28]J.-K. Lee, S.-C. Lee, J.-P. Ahn, S.-C. Kim, J. I. B. Wilson, and P. John, J. Chem. Phys. **129**, 234709 (2008).
[29]See supplementary material at http://dx.doi.org/10.1063/1.4802881 for methods and TEM images of commercial MWNTs prepared by the vapor phase catalytic chemical vapour deposition technique and an arc-discharge technique (Fig. S1); the crystal structure of AB graphite (Fig. S2); expected ED patterns of a turbostratic MWNT if it exists (Fig. S3); an expected ED pattern of an armchair MWNT if it exists (Fig. S4); and AFM analysis of a CVD-MWNT (Fig. S5).
[30]Y. Imai and A. Watanabe, J. Alloys Compd. **439**, 258 (2007).
[31]F. Izumi and K. Momma, Solid State Phenom. **130**, 15 (2007).
[32]Z. Xin, Z. Jianjun, and O.-Y. Zhong-can, Phys. Rev. B **62**, 13692 (2000).
[33]R. A. Segura, W. Ibáñez, R. Soto, S. Hevia, and P. Häberle, J. Nanosci. Nanotechnol. **6**, 1945 (2006).
[34]B. Louis, G. Gulino, R. Vieira, J. Amadou, T. Dintzer, S. Galvagno, G. Centi, M. J. Ledoux, and C. Pham-Huu, Catal. Today **102–103**, 23 (2005).
[35]L. P. Biró, Z. E. Horváth, A. A. Koós, Z. Osváth, Z. Vértesy, Al. Darabont, K. Kertész, C. Neamtu, Zs. Sárkoözi, and L. Tapasztó, J. Optoelectron. Adv. Mater. **5**, 661 (2003).
[36]D. Zhang, L. Shi, J. Fang, K. Dai, and X. Li, Mater. Chem. Phys. **97**, 415 (2006).
[37]A. Huczko, Appl. Phys. A **74**, 617 (2002).
[38]N. Bajawa, X. Li, P. M. Ajayan, and R. Vajtai, J. Nanosci. Nonotechnol. **8**, 6054 (2008).
[39]X. Sun, R. Li, B. Stansfield, J.-P. Dodelet, G. Menard, and S. Desilets, Carbon **45**, 732 (2007).
[40]W. Li, S. Xie, W. Liu, R. Zhao, Y. Zhang, W. Zhou, and G. Wang, J. Mater. Sci. **34**, 2715 (1999).
[41]S. Amelinckx, X. B. Zhang, D. Bernaerts, X. F. Zhang, V. Lvanov, and J. B. Nagy, Science **265**, 635 (1994).
[42]N. Wang, K. K. Fung, W. Lu, and S. Yang, Chem. Phys. Lett. **229**, 587 (1994).
[43]H.-L. Zhang, J.-F. Li, B.-P. Zhang, K.-F. Yao, W.-S. Liu, and H. Wang, Phys. Rev. B **75**, 205407 (2007).
[44]J.-P. Salvetat, J.-M. Bonard, N. H. Thomson, A. J. Kulik, L. Forró, W. Benoit, and L. Zuppiroli, Appl. Phys. A **69**, 255 (1999).
[45]J.-K. Lee, S. Lee, Y.-I. Kim, J.-G. Kim, J.-P. Ahn, K.-I. Lee, S.-H. Jeong, and P. John, "A mechanical route to graphene nanoribbons," (unpublished).
[46]J. Biscoe and B. E. Warren, J. Appl. Phys. **13**, 364 (1942).
[47]R. L. V. Wal, A. J. Tomasek, M. I. Pamphlet, C. D. Taylor, and W. K. Thompson, J. Nanopart. Res. **6**, 555 (2004).